Bismuth(III)-Catalysed Hydroalkylation of Styrene with Acetylacetone: A DFT-Based Mechanistic Study

Mona Jalali,[a] Farshad Shiri,[b] Alex C. Bissember,[a] Brian F. Yates[a]* and Alireza Ariafard[a]*

[a]*School of Natural Sciences – Chemistry, University of Tasmania, Hobart, Tasmania 7001, Australia;* [b]*Department of Chemistry, Islamic Azad University, Central Tehran Branch, Poonak, Tehran 1469669191, Iran*

Correspondence details:

Brian F. Yates, Brian.Yates@utas.edu.au

Alireza Ariafard, Alireza.Ariafard@utas.edu.au

ORCID

Mona Jalali, http://orcid.org/0000-0001-9705-2816

Farshad Shiri, http://orcid.org/0000-0001-5838-5007

Alex C. Bissember, http://orcid.org/0000-0001-5515-2878

Brian F. Yates, http://orcid.org/0000-0001-9663-3301

Alireza Ariafard, http://orcid.org/0000-0003-2383-6380

Received date:

Word count: 5221

Bismuth(III)-Catalysed Hydroalkylation of Styrene with Acetylacetone: A DFT-Based Mechanistic Study

Abstract: Density functional theory (DFT) has been used to investigate the mechanism of the experimentally efficient hydroalkylation of styrene with acetylacetone in the presence of a bismuth catalyst. It is shown that the mechanism is fundamentally different to that of the analogous gold-catalysed reaction, even though it leads to the same product. Whereas gold prefers to coordinate to the π-bond of the enol isomer of acetylacetone, bismuth coordinates to the two oxygens to form a chelated complex. Furthermore, the overall reaction with bismuth via the enol isomer of acetylacetone occurs with a much lower activation energy compared to the ketone isomer. In addition, several bismuth catalysts were considered and two of these were shown to have no activity. All of these results have been rationalised in terms of the strength of binding of the metal centres to the acetylacetone. The stronger the binding, the greater the acidity of a proton on acetylacetone, and thus the lower the activation energy for the protonation of styrene, which turns out to be the rate-determining step in the overall reaction. In this way, good agreement is obtained with all the experimental data.

Keywords: density functional theory (DFT); Bismuth(III) catalysis, reaction mechanism, acetylacetone, hydroalkylation, styrene

Introduction

Hydroalkylation via metal-catalysed C–H functionalisation remains a powerful tool for building molecular complexity in organic synthesis [1-4]. For example, Rueping and coworkers developed a method for hydroalkylation of alkenes via the intermolecular addition of 1,3-dicarbonyl molecules (acetylacetone) to styrene derivatives catalysed by $Bi(OTf)_3(H_2O)_4$ [5]. These researchers found that heating acetylacetone (**1**) with styrene (**2**) in nitromethane at 80 °C in the presence of $Bi(OTf)_3(H_2O)_4$ delivered coupled product **3** efficiently after 2 h (Table 1, entry 1). Interestingly, it was observed that this transformation could not be facilitated by other bismuth salts, such as $BiCl_3$ and $BiBr_3$ (entries 2 and 3). This indicated that triflate ligands play a key role in the reactivity of the bismuth catalyst. These

experimental findings may derive from the greater Lewis acidity of $Bi(OTf)_3$ relative to $BiCl_3$ and $BiBr_3$ [6-10]. However, a mechanistic proposal was not reported by Rueping and coworkers in their original study.

[Table 1 near here]

Many hydroalkylation reactions of alkenes with substrates bearing activated methylene moieties have been developed under Lewis and Brønsted acid catalysis and associated mechanistic studies have been undertaken [11-19]. In germane studies, Ariafard and coworkers [20] recently employed DFT to investigate the mechanism of the reaction of acetylacetone with styrene catalysed by $AuCl_3$/AgOTf that was first developed Li and coworkers [11], (Scheme 1). These DFT studies revealed that highly electron deficient complex $Au(OTf)_3$ is strongly bound to the C=C π-bond of the enol tautomer of acetylacetone, which increases the acidity of the OH proton within enol **1′** (Scheme 1b). Styrene then deprotonates the most acidic proton within enol **1′** to generate a benzylic carbocation. Notably, it is this free carbocation that actually serves as the active catalyst and mediates the hydroalkylation reaction via the proposed cycle shown in Scheme 1.

[Scheme 1 near here]

The above-mentioned results prompted us to employ computational methods to investigate whether the role of $Bi(OTf)_3$ as a hydroalkylation catalyst is similar to $Au(OTf)_3$. Although both metal centres bear +3 oxidation states, the former is a main group metal, while the latter is a transition metal. Specifically, through this study we aimed to address the following questions: 1) Does the hydroalkylation facilitated by the Bi(III) complex proceed via an analogous benzylic carbocation mechanism? 2) If not, what could be the mechanism for such a reaction? 3) Why, in contrast to $Bi(OTf)_3(H_2O)_4$, are bismuth halides ($BiCl_3$ and $BiBr_3$) ineffective hydroalkylation catalysts?

This study employs DFT calculations to address these questions and enhance fundamental understanding of hydroalkylation processes, more broadly.

Computational methods

Gaussian 16 [22] was used to fully optimise all the structures reported in this paper at the M06-2X level of density functional theory (DFT) [23-25]. For all the calculations, solvent effects were considered using the SMD solvation model for CH_3NO_2 solvent [26]. The effective core potential of Hay and Wadt with a double-ξ valence basis set (LANL2DZ) [27-28] was chosen to describe bismuth. Polarisation functions were also added for Bi (ξd= 0.202) [29]. The 6-31G(d) basis set was used for other atoms [30]. This basis set combination will be referred to as BS1. Frequency calculations were carried out at the same level of theory as those for the structural optimisation. Transition structures were located using the Berny algorithm. Intrinsic reaction coordinate (IRC) calculations [31-32] were used to confirm the connectivity between transition structures and minima. To further refine the energies obtained from the SMD/M06-2X /BS1 calculations, we carried out single-point energy calculations using the M06-2X functional method [33] for all the structures with a larger basis set (BS2). BS2 utilises the def2-TZVP [34] basis set on all atoms. Tight convergence criterion was also employed to increase the accuracy of the single point calculations. All thermodynamic data were calculated at the standard state (298.15 K and 1 atm).

In this work, the free energy for each species optimised by SMD/M06-2X/BS1 in solution was calculated using the formula: G = E(BS2) + G(BS1) – E(BS1) + ΔG 1atm→1M; where ΔG 1atm→1M = 1.89 kcal/mol is the free-energy change for compression of 1 mole of an ideal gas from 1 atm to the 1 M solution phase standard state. Natural bond orbital (NBO) and natural localised molecular orbital (NLMO) analyses were carried out using NBO7 software integrated with Gaussian 16 [35]. Second-generation energy decomposition analysis

(EDA) based on absolutely localised molecular orbitals (ALMO-EDA2) was implemented in Q-Chem 5.2 [36] carried out at the SMD/M06L-D3/def2-TZVP level of theory.

Results and discussion

We began our DFT investigation by determining the stability of the possible isomers of the experimental catalyst $Bi(OTf)_3(H_2O)_4$ (Figure 1). The seven-coordinate complex $Bi(OTf)_3(H_2O)_4$ (**4**) is predicted to exhibit pentagonal bipyramidal metal coordination geometry [21] (Figure 1a, structure **4**). The stability of complex **4** was also compared to that of other possible outer sphere complexes in which the six coordinate complex $Bi(OTf)_3(H_2O)_3$ is stabilised by hydrogen bonding interactions with the fourth water molecule (complexes **5**–**7**). This comparison shows that the pentagonal bipyramid structure **4** is more stable than outer-sphere complexes **5**–**7**. The calculations revealed that structure **4** can be easily converted to octahedral complex **8** by dissociating one water molecule in a nearly thermoneutral manner (Figure 1b).

[Figure 1 near here]

The facial (*fac*) octahedral complex **8** can isomerise to the meridional (*mer*) complex **9** (Figure 2a). Our calculations indicate that these two geometrical isomers are nearly identical in terms of stability, with the *fac* isomer being lower in energy by 1.3 kcal/mol. In both isomers (Figure 2a), a coordinated water molecule forms a hydrogen bond with a pendant oxygen atom of a triflate ligand. As shown in Figure 2a, the Bi–OTf bonds are shorter than the $Bi–OH_2$ bonds in both isomers, implying that triflate is a more effective donor ligand than water. The slightly lower stability of the *mer* isomer compared to the *fac* isomer can be explained by the destabilizing *trans*-positioning of two triflate ligands having rather strong σ donor character.

Both isomers **8** and **9** are shown to have a low reactivity toward the dissociation of a triflate ligand, which is supported by the significant endergonicity calculated for this process (Figure **2**b). In contrast, the free energies of reaction for the dissociation of water from isomers **8** and **9** are computed to be ~ 2 kcal/mol. This suggests that the water molecule is a good leaving group, readily providing an empty coordination site for binding acetylacetone.

[Figure 2 near here]

Benzylic carbocation mechanism

We next investigated how feasible the benzylic carbocation mechanism (Scheme 1) is for the hydroalkylation reaction catalysed by $Bi(OTf)_3(H_2O)_4$. Figure 3 depicts the energy profile for the formation of the key benzylic carbocation, which occurs via coordination of the C=C π-bond of the enol tautomer to the coordinatively unsaturated species **10**, yielding π-complex **14**. The ensuing π-complex then protonates the styrene via transition structure $\mathbf{TS_{14\text{-}15}}$ with a relative free energy as high as 39.2 kcal/mol. Figure 3 also shows another pathway for protonation of the styrene. Specifically, this involves the dissociation of water from **14** to form complex **17** in which the enol tautomer acts as a bidentate ligand. The deprotonation from resultant complex **17** via transition structure $\mathbf{TS_{17\text{-}18}}$ requires a very high activation barrier ($\Delta G^{\ddagger}$ = 37.8 kcal/mol). The benzylic carbocation mechanism was also investigated for the case in which the enol form of acetylacetone coordinates to the coordinatively unsaturated complex **12** (Figure 4). Again, we found an extremely high activation barrier was required for π-complexes **19** and **21** to protonate styrene. These findings indicate that the benzylic carbocation mechanism is unlikely to operate in the hydroalkylation reaction catalysed by $Bi(OTf)_3(H_2O)_4$.

We wanted to understand why the benzylic carbocation mechanism is feasible for the $Au(OTf)_3$-catalysed reaction, but is unfeasible in the presence of $Bi(OTf)_3(H_2O)_4$. As

illustrated in Figure 5a, the coordination of the enol to the Bi(III) centre via its C=C π-bond to form **14** is endergonic (+11.8 kcal/mol). In comparison, the coordination to the Au(III) centre is calculated to be exergonic (–30.4 kcal/mol). An inspection of optimised structures for π-complexes Bi **14** and Au **17'** indicates that the respective M–C^1 and M–C^2 bond distances are longer within the former than the latter. NBO analysis for these two structures also reveals that the Wiberg bond indexes (WBIs) for the M–C^1 and M–C^2 bonds are smaller when M = Bi (Figure 5b). Thus, it follows that the interaction between the Bi(III) centre and the C=C π-bond of the enol tautomer is quite weak, while it is strong between the Au(III) and the enol. This means that the metal centres within the Bi(III) complexes have a very poor π-philic character. Due to the weak π-coordination of the enol to the Bi centre, the OH proton of the coordinated enol is not sufficiently acidic, which is consistent with deprotonation by styrene requiring a very high activation barrier.

A comparison of the electronic structures of **17″** and **14** using the natural localized molecular orbital (NLMO) method reveals that the bond between the enol tautomer and the gold atom in **17″** has more covalent character than the bond between the enol tautomer and the bismuth atom in **14** (Figure 5c). This is supported by significant contributions of Au (38.7%) to the Au–enol bond in complex **17''**. In contrast, the contribution of Bi (11.2%) to the Bi–enol bond is significantly smaller than the contributions of C1 and C2 (70.5% + 10.2% = 80.7%), implying a weaker covalent interaction between bismuth and enol in complex **14**. To further substantiate the findings of the NLMO analysis, we evaluated the bonding in these two complexes using the second-generation energy decomposition analysis (EDA) based on absolutely localised molecular orbitals (ALMO-EDA2) implemented in Q-Chem 5.2 (for details see Table S1). According to EDA calculations, orbital interactions play a crucial role in the π-bond strength of these complexes; ΔE_{orb} for interaction between the enol and the metal centres are calculated to be –129.3 and –54.4 kcal/mol in **17''** and **14**,

respectively. The calculations show that the interaction of the enol C=C π orbital with the Au(III) $d_{x^2-y^2}$ orbital in **17''** or with a Bi(III) p orbital in **14** is the primary source of orbital interactions, supported by the contour plots of natural orbitals for chemical valence (NOCV) for these complexes (Figure 5d); the corresponding interaction is calculated to be more significant in **17''** (–106.4 kcal/mol) than that in **14** (–43.9 kcal/mol).

[Figure 3 near here]

[Figure 4 near here]

[Figure 5 near here]

Other mechanisms

The foregoing results demonstrate that the hydroalkylation catalysed by $Bi(OTf)_3(H_2O)_4$ proceeds via a different mechanism to the analogous process in the presence of $Au(OTf)_3$. Scheme 2 outlines four different plausible reaction pathways (1–4) that may account for this transformation. In these reaction pathways, the ketone or enol form of acetylacetone binds to the Bi atom of the *fac*- or *mer*-isomer as a bidentate ligand through its oxygen atoms. This leads to four different chelate complexes **25**, **29**, **33**, and **35**. In these complexes, the coordinated acetylacetone serves as an acid, protonating the styrene to produce ion pairs **26** and **30**. Finally, the most nucleophilic carbon atom of the acetylacetonate (acac) ligand adds to the benzylic cation via transition structures $\mathbf{TS_{26\text{-}27}}$ and $\mathbf{TS_{30\text{-}31}}$ to furnish hydroalkylation product **3**.

[Scheme 2 near here]

Scheme 3 compares the stability of the chelate complexes (**25**, **29**, **33**, **35)** to *π*-complex **14**. This comparison indicates that the chelated complexes are much more stable than the *π*-complex. The stronger oxophilicity of the Bi(III) centre than its π-philicity may account for the increased stability of the chelate complexes. When the metal centre is

changed from Bi(III) to Au(III), the stability sequence is reversed (Figure 3). This means that, in contrast to the Bi(III) atom, the Au(III) atom exhibits greater π-philicity than oxophilicity. This feature might explain why the hydroalkylation proceeds via a different mechanism when the catalyst is switched from $Au(OTf)_3$ to $Bi(OTf)_3(H_2O)_4$ (*vide infra*).

[Scheme 3 near here]

Figure 6 depicts the computed energy profiles for the four pathways shown in Scheme 2. A number of conclusions can be drawn after careful examination of the energy profiles. (1) The rate-determining step in all pathways is computed to be the styrene-induced deprotonation of the chelate complexes. (2) The protonation of styrene by chelate complexes with the coordinated enol tautomer requires lower activation barriers than protonation by chelate complexes with the coordinated ketone tautomer; both transition structures **TS$_{33\text{-}26}$** and **TS$_{35\text{-}30}$** are substantially lower in energy than transition structures **TS$_{25\text{-}26}$** and **TS$_{29\text{-}30}$**. This indicates that the coordinated enol form contains a proton that is more acidic than the coordinated ketone form [37]. A plausible reason for this is that the proton in the enol form is bound to the oxygen atom, which is more electronegative than the carbon atom to which the acidic proton is bound in the ketone form. (3) The *mer* isomer was found to be slightly more reactive than the *fac* isomer as evidenced by the fact that **TS$_{35\text{-}30}$** lies lower in energy than **TS$_{33\text{-}26}$**.

[Figure 6 near here]

Figure 7 presents the catalytic cycle proposed by the DFT calculations for $Bi(OTf)_3(H_2O)_4$-catalysed hydroalkylation of styrene with acetylacetone. The cycle begins with the dissociation of two water molecules from **4** to give coordinatively unsaturated species **12′**. Subsequently, the enol tautomer of acetylacetone coordinates to the Bi centre in **12′**, yielding complex **35** in which the OH proton of the coordinated enol becomes sufficiently acidic that the styrene can deprotonate it to give ion pair **30**. The resulting ion

pair is extremely reactive towards carbon–carbon coupling, leading to formation of the product coordinated to the Bi atom in **31**. Finally, a ligand exchange between **31** and the enol tautomer of acetylacetone occurs, releasing the hydroalkylation product and regenerating active catalyst **35**.

[Figure 7 near here]

Hydroalkylation by other bismuth catalysts

As mentioned in the Introduction, $BiCl_3$ and $BiBr_3$ are inefficient catalysts for the hydroalkylation of styrene. To explain why this is the case, we calculated the styrene-induced protonation step using $BiCl_3$ and $BiBr_3$ as the Lewis acid catalyst through five distinct pathways, as shown in Table 2. Consistent with the experimental findings, in each of these five pathways we found that this crucial step is highly energy demanding ($\Delta G^{\ddagger} > 34$ kcal/mol). This reveals that, in comparison to $Bi(OTf)_3(H_2O)_4$, neither $BiCl_3$ nor $BiBr_3$ is acidic enough to sufficiently activate the coordinated acetylacetone towards deprotonation by styrene. Indeed, the Bi–OH bond within intermediates **39-Cl** and **39-Br** is much longer than that in **33** (Figure 8). This indicates that the OH group of the enol tautomer does not interact strongly enough with $BiCl_3$ and $BiBr_3$, resulting in it not becoming sufficiently acidic to carry out the protonation process with a low barrier. It follows from these results that a suitably acidic Bi catalyst is required to promote this hydroalkylation process.

[Table 2 near here]

[Figure 8 near here]

Conclusions

In summary, our computational investigation reveals that the mechanism for the hydroalkylation of styrene with $Bi(OTf)_3(H_2O)_4$ is fundamentally different to the mechanism

for the analogous reaction with $AuCl_3$/AgOTf. Whereas gold prefers to coordinate to the π-bond of the enol from of acetylacetone, bismuth coordinates to the two oxygens to form a chelated complex. Furthermore, when the enol and ketone forms of acetylacetone are compared in the reaction with bismuth, it is found that the overall reaction with the enol form occurs with a much lower activation energy than the ketone form. In addition, we have shown that reactions employing either $BiCl_3$ or $BiBr_3$ require very large energies of activation, which is consistent with their inability to serve as hydroalkylation catalysts experimentally. All of these results can be rationalised in terms of the strength of binding of the metal centres to acetylacetone. The stronger the binding, the greater the acidity of either an enolic or α-proton on acetylacetone, and thus the lower the activation energy for the protonation of styrene, which turns out to be the rate-determining step in the overall reaction. This rationalisation provides good agreement with the available experimental data. Finally, we note that although the bismuth- and gold-catalysed reactions proceed via different mechanisms, the lowest energy pathways have similar calculated activation energies [20] and this agrees well with experimental observations that similar temperatures are required for both processes.

Acknowledgments

We thank the Australian Research Council (ARC) for project funding (DP180100904) and the Australian National Computational Infrastructure and the University of Tasmania for the generous allocation of computing time. A.C.B.'s contributions were supported by an ARC Future Fellowship (FT200100049). B.F.Y. wishes to acknowledge the friendship, inspiring conversations since PhD days and the many significant contributions to computational chemistry by Peter Gill, and wishes him all the best for his 60th birthday.

Disclosure statement

The authors report there are no competing interests to declare.

Data availability statement

Supplemental Material (free energy reaction profiles, Cartesian coordinates and calculated energies for all species discussed in this work) is available via the Molecular Physics journal website.

References

[1] Li, C. J., Organic Reactions in Aqueous Media—With a Focus on Carbon-Carbon Bond Formation. *Chem. Rev.* **1993,** *93*, 2023-2035.

[2] Dyker, G., Transition Metal Catalyzed Coupling Reactions under C−H Activation. *Angew. Chem. Int. Ed.* **1999,** *38*, 1698-1712.

[3] Trost, B., The Atom Economy—A Search for Synthetic Efficiency. *Science* **1991,** *254*, 1471-1477.

[4] Ren, T.; Patel, M.; Blok, K., Olefins from conventional and heavy feedstocks: Energy use in steam cracking and alternative processes. *Energy.* **2006,** *31*, 425-451.

[5] Rueping, M.; Nachtsheim, B. J.; Kuenkel, A., An Efficient Metal-Catalyzed Hydroalkylation. *Synlett* **2007,** *9*, 1391-1394.

[6] Gaspard-Iloughmane, H.; Le Roux, C., Bismuth(III) Triflate in Organic Synthesis. *Eur. J. Org. Chem.* **2004**, 25172532.

[7] Banerjee, B., Bismuth(III) triflate: An Efficient Catalyst for the Synthesis of Diverse Biologically Relevant Heterocycles. *ChemistrySelect* **2017,** *2*, 6744 – 6757.

[8] Bothwell, J. M.; Krabbe, S. W.; Mohan, R. S., Applications of bismuth(III) compounds in organic synthesis. *Chem. Soc. Rev.* **2011,** *40*, 4649–4707.

[9] Le Roux, C.; Dubac, J., Bismuth(III) Chloride and Triflate: Novel Catalysts for Acylation and Sulfonylation Reactions. Survey and Mechanistic Aspects. *Synlett* **2002,** *2*, 181–200.

[10] Babaahmadi, R.; Jalali, M.; Smith, J. A.; Yates, B. F.; Ariafard, A., How a Bismuth(III) Catalyst Achieves Greatest Activation of Organic Lewis Bases in a Catalytic Reaction: Insights from DFT Calculations. *ChemCatChem* **2021,** *13*, 975–980.

[11] Yao, X.; Li, C.-J., Highly Efficient Addition of Activated Methylene Compounds to Alkenes Catalyzed by Gold and Silver. *J. Am. Chem. Soc.* **2004,** *126*, 6884-6885.

[12] Duan, Z.; Xuan, X.; Wu, Y., FeCl3 Catalyzed Addition of Activated Methylenes to Styrene Derivatives under Air. *Tetrahedron Lett.* **2007,** *48*, 5157−5159. .

[13] Li, Y.; Yu, Z.; Wu, S., Efficient Copper(II)-Catalyzed Addition of Activated Methylene Compounds to Alkenes. *J. Org. Chem.* **2008,** *73*, 5647−5650. .

[14] Yuan, Y.; Shi, Z., Indium(III)-Catalyzed Addition of 1,3-Dicarbonyl Compounds to Alkenes. *Synlett* **2007**, 3219−3223.

[15] Wang, H. S.; Zhao, W. X., Magnesium Bistrifluoromethanessulfonimide as an Efficient Catalyst for the Hydroalkylation of Aromatic Olefins with 1,3-diketones under Solvent-free Conditions. *Chin. Chem. Lett.* **2011,** *22*, 911-914.

[16] Shimizu, K.-i. Y., T.; Tai, Y.; Okumura, K.;; Satsuma, A., Addition of Olefins to Acetylacetone Catalyzed by Cooperation of Bronsted Acid Site of Zeolite and Gold Cluster. *Appl. Catal. A.* **2011,** *400*, 171-175.

[17] Nguyen, R.-V.; Yao, X.; Li, C.-J., Highly Efficient Gold-Catalyzed Atom-Economical annulation of Phenols with dienes. *Org. Lett.* **2006,** *8*, 2397−2399.

[18] Meng, G.; Patel, M.; Luo, F.; Li, Q.; Flach, C.; Mendelsohn, R.; Garfunkel, E.; He, H.; Szostak, M., Graphene Oxide Catalyzed Ketone α-alkylation with Alkenes: Enhancement of Graphene Oxide Activity by Hydrogen Bonding. *Chem. Commun.* **2019,** *55*, 5379−5382.

[19] Lanman, H. E.; Nguyen, R.-V.; Yao, X.; Chan, T.-H.; Li, C.-J., Evaluating Lewis Acid Catalyzed Hydroalkylation of Alkenes in Neat and in Ionic Liquids. *J. Mol. Catal. A: Chem.* **2008,** *279*, 218−222.

[20] Jalali, M.; Hyland, C. J. T.; Bissember, A. C.; Yates, B. F.; and Ariafard, A., Hydroalkylation of Alkenes with 1,3-Diketones via Gold(III) or Silver(I) Catalysis: Divergent Mechanistic Pathways Revealed by a DFT-Based Investigation. *ACS Catal.* **2021,** *11*, 5795−5807.

[21] Dudev, M. W., J.; Dudev, T.; Lim, C., Factors Governing the Metal Coordination Number in Metal Complexes from Cambridge Structural Database Analyses. *J. Phys. Chem. B* **2006,** *110*, 1889-1895.

[22] Frisch, M. J.; Trucks, G. W.; Schlegel, H. B.; Scuseria, G. E.; Robb, M. A.; Cheeseman, J. R.; Scalmani, G.; Barone, V.; Petersson, G. A.; Nakatsuji, H.; Li, X.; Caricato, M.; Marenich, A. V.; Bloino, J.; Janesko, B. G.; Gomperts, R.; Mennucci, B.; Hratchian, H. P.; Ortiz, J. V.; Izmaylov, A. F.; Sonnenberg, J. L.; Williams-Young, D.; Ding, F.; Lipparini, F.; Egidi, F.; Goings, J.; Peng, B.; Petrone, A.; Henderson, T.; Ranasinghe, D.; Zakrzewski, V. G.; Gao, J.; Rega, N.; Zheng, G.; Liang, W.; Hada, M.; Ehara, M.; Toyota, K.; Fukuda, R.; Hasegawa, J.; Ishida, M.;

Nakajima, T.; Honda, Y.; Kitao, O.; Nakai, H.; Vreven, T.; Throssell, K.; Montgomery, J. A.; Peralta, J. E.; Ogliaro, F.; Bearpark, M. J.; Heyd, J. J.; Brothers, E. N.; Kudin, K. N.; Staroverov, V. N.; Keith, T. A.; Kobayashi, R.; Normand, J.; Raghavachari, K.; Rendell, A. P.; Burant, J. C.; Iyengar, S. S.; Tomasi, J.; Cossi, M.; Millam, J. M.; Klene, M.; Adamo, C.; Cammi, R.; Ochterski, J. W.; Martin, R. L.; Morokuma, K.; Farkas, O.; Foresman, J. B.; and Fox, D. J. *Gaussian 16*, Revision B.01 (Gaussian, Inc., Wallingford CT, 2016).

[23] Lee, C.; Yang, W.; Parr, R. G., Development of the Colle-Salvetti Correlation-energy Formula into a Functional of the Electron Density. *Phys. Rev. B.* **1988,** *37*, 785−789.

[24] Miehlich, B.; Savin, A.; Stoll, H.; Preuss, H., Results Obtained with the Correlation Energy Density Functionals of Becke and Lee, Yang and Parr. *Chem. Phys. Lett* **1989,** *157*, 200−206.

[25] Becke, A. D. J., Density Functional Thermochemistry. III. The Role of Exact Exchange. *Chem. Phys. Lett* **1993,** *98*, 5648−5652.

[26] Marenich, A. V.; Cramer, C. J.; Truhlar, D. G., Universal Solvation Model Based on Solute Electron Density and on a Continuum Model of the Solvent Defined by the Bulk Dielectric Constant and Atomic Surface Tensions. *J. Phys. Chem. B* **2009,** *113*, 6378-6396.

[27] Wadt, W. R.; Hay, P. J., Ab initio Effective Core Potentials for Molecular Calculations. Potentials for Main Group elements Na to Bi. *J. Chem. Phys.* **1985,** *82*, 284−298.

[28] Hay, P. J.; Wadt, W. R., Ab initio Effective Core Potentials for Molecular Calculations. Potentials for the Transition Metal Atoms Sc to Hg. *J. Chem. Phys.* **1985,** *82*, 270−283. .

[29] Ehlers, A. W.; Böhme, M.; Dapprich, S.; Gobbi, A.; Höllwarth, A.; Jonas, V.; Köhler, K. F.; Stegmann, R.; Veldkamp, A.; Frenking, G., A Set of f-polarization Functions for Pseudo-potential Basis Sets of the Transition Metals Sc-Cu, Y-Ag, La-Au. *Chem. Phys. Lett.* **1993,** *208*, 111−114.

[30] Hariharan, P. C.; Pople, J. A., The Influence of Polarization Functions on Molecular Orbital Hydrogenation Energies. *Theoret. Chim. Acta.* **1973,** *28*, 213−222.

[31] Fukui, K., The Path of Chemical Reactions - The IRC Approach. *Acc. Chem. Res.* **1981,** *14*, 363−368.

[32] Fukui, K., A Formulation of the Reaction Coordinate. *Phys. Chem.* **1970,** *74*, 4161–4163.

[33] Zhao, Y.; Truhlar, D. G., Density Functionals with Broad Applicability in Chemistry. *Acc. Chem. Res.* **2008,** *41*, 157−167.

[34] Weigend, F.; Furche, F.; Ahlrichs, R., Gaussian Basis Sets of Quadruple Zeta Valence Quality for Atoms H-Kr. *Chem. Phys. Lett.* **2003,** *119*, 12753–12762.

[35] Glendening, E. D.; Badenhoop, J. K.; Reed, A. E.; Carpenter J. E.; Bohmann, J. A.; Morales, C. M.; Landis, C. R.; Weinhold, F., *Natural Bond Order 6.0* (Theoretical Chemistry Institute, University of Wisconsin, Madison, WI, 2013).

[36] Shao, Y.; Gan, Z.; Epifanovsky, E.; Gilbert, A. T. B.; Wormit, M.; Kussmann, J.; Lange, A. W.; Behn, A.; Deng, J.; Feng, X.; Ghosh, D.; Goldey, M.; Horn, P. R.; Jacobson, L. D.; Kaliman, I.; Khaliullin, R. Z.; Kus, T.; Landau, A.; Liu, J.; Proynov, E. I.; Rhee, Y. M.; Richard, R. M.; Rohrdanz, M. A.; Steele, R. P.; Sundstrom, E. J.; Woodcock, H. L.; Zimmerman, P. M.; Zuev, D.; Albrecht, B.; Alguire, E.; Austin, B.; Beran, G. J. O.; Bernard, Y. A.; Berquist, E.; Brandhorst, K.; Bravaya, K. B.; Brown, S. T.; Casanova, D.; Chang, C.-M.; Chen, Y.; Chien, S. H.; Closser, K. D.; Crittenden, D. L.; Diedenhofen, M.; DiStasio, R. A.; Do, H.; Dutoi, A. D.; Edgar, R. G.; Fatehi, S.; FustiMolnar, L.; Ghysels, A.; Golubeva-Zadorozhnaya, A.; Gomes, J.; Hanson-Heine, M. W. D.; Harbach, P. H. P.; Hauser, A. W.; Hohenstein, E. G.; Holden, Z. C.; Jagau, T.-C.; Ji, H.; Kaduk, B.; Khistyaev, K.; Kim, J.; Kim, J.; King, R. A.; Klunzinger, P.; Kosenkov, D.; Kowalczyk, T.; Krauter, C. M.; Lao, K. U.; Laurent, A. D.; Lawler, K. V.; Levchenko, S. V.; Lin, C. Y.; Liu, F.; Livshits, E.; Lochan, R. C.; Luenser, A.; Manohar, P.; Manzer, S. F.; Mao, S.-P.; Mardirossian, N.; Marenich, A. V.; Maurer, S. A.; Mayhall, N. J.; Neuscamman, E.; Oana, C. M.; Olivares-Amaya, R.; O'Neill, D. P.; Parkhill, J. A.; Perrine, T. M.; Peverati, R.; Prociuk, A.; Rehn, D. R.; Rosta, E.; Russ, N. J.; Sharada, S. M.; Sharma, S.; Small, D. W.; Sodt, A.; Stein, T.; Stück, D.; Su, Y.-C.; Thom, A. J. W.; Tsuchimochi, T.; Vanovschi, V.; Vogt, L.; Vydrov, O.; Wang, T.; Watson, M. A.; Wenzel, J.; White, A.; Williams, C. F.; Yang, J.; Yeganeh, S.; Yost, S. R.; You, Z.-Q.; Zhang, I. Y.; Zhang, X.; Zhao, Y.; Brooks, B. R.; Chan, G. K. L.; Chipman, D. M.; Cramer, C. J.; Goddard, W. A.; Gordon, M. S.; Hehre, W. J.; Klamt, A.; Schaefer, H. F.; Schmidt, M. W.; Sherrill, C. D.; Truhlar, D. G.; Warshel, A.; Xu, X.; Aspuru-Guzik, A.; Baer, R.; Bell, A. T.; Besley, N. A.; Chai, J.-D.; Dreuw, A.; Dunietz, B. D.; Furlani, T. R.;

Gwaltney, S. R.; Hsu, C.-P.; Jung, Y.; Kong, J.; Lambrecht, D. S.; Liang, W.; Ochsenfeld, C.; Rassolov, V. A.; Slipchenko, L. V.; Subotnik, J. E.; Van Voorhis, T.; Herbert, J. M.; Krylov, A. I.; Gill, P. M. W.; Head Gordon, M., Advances in molecular quantum chemistry contained in the Q-Chem 4 program package. *Mol. Phys.* **2015**, *113*, 184−215.

[37] An internal hydrogen bond is identified in complex **33** with a distance of 1.604 Å between the OH enol ligand and an OTf ligand. However, this interaction is not strong enough to prevent the proton transfer to styrene via **TS$_{33\text{-}26}$** with $\Delta G^{\ddagger}$ 22.3 kcal/mol (Figure 6c). We can also rule out the reaction proceeding from **33** via an internal proton transfer to an OTf ligand followed by the release of HOTf for two reasons. Firstly, it has been shown experimentally that HOTf does not catalyse the reaction (ref. 5). Secondly, because a recent computational study of a related bismuth reaction shows that this possibility is a highly endergonic process (ref. 10).

Table 1. Bismuth-catalysed intermolecular hydroalkylation reaction of styrene (**2**) with acetylacetone (**1**) reported by Rueping and coworkers.

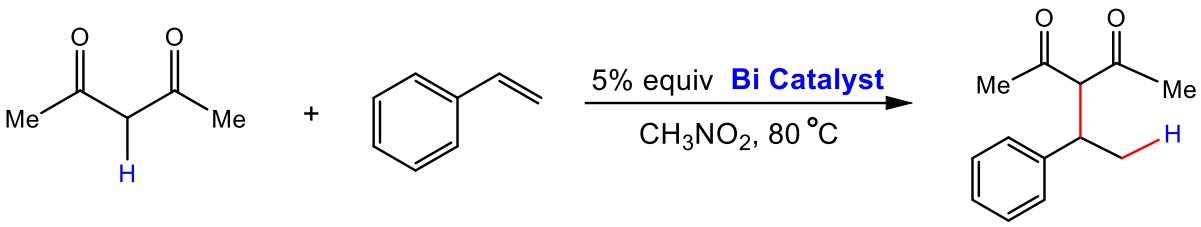

1 **2** **3**

Entry	Catalyst	time (h)	yield (%)
1	$Bi(OTf)_3(H_2O)_4$	2	81
2	$BiCl_3$	8	0
3	$BiBr_3$	8	0

Table 2. Calculated free energy barrier for styrene-induced protonation step using $BiCl_3$ and $BiBr_3$. Free energies calculated by SMD/M06-2X/def2-TZVP//SMD/M06-2X/LANL2DZ(d),6-31G(d) level of theory in nitromethane are given in kcal/mol.

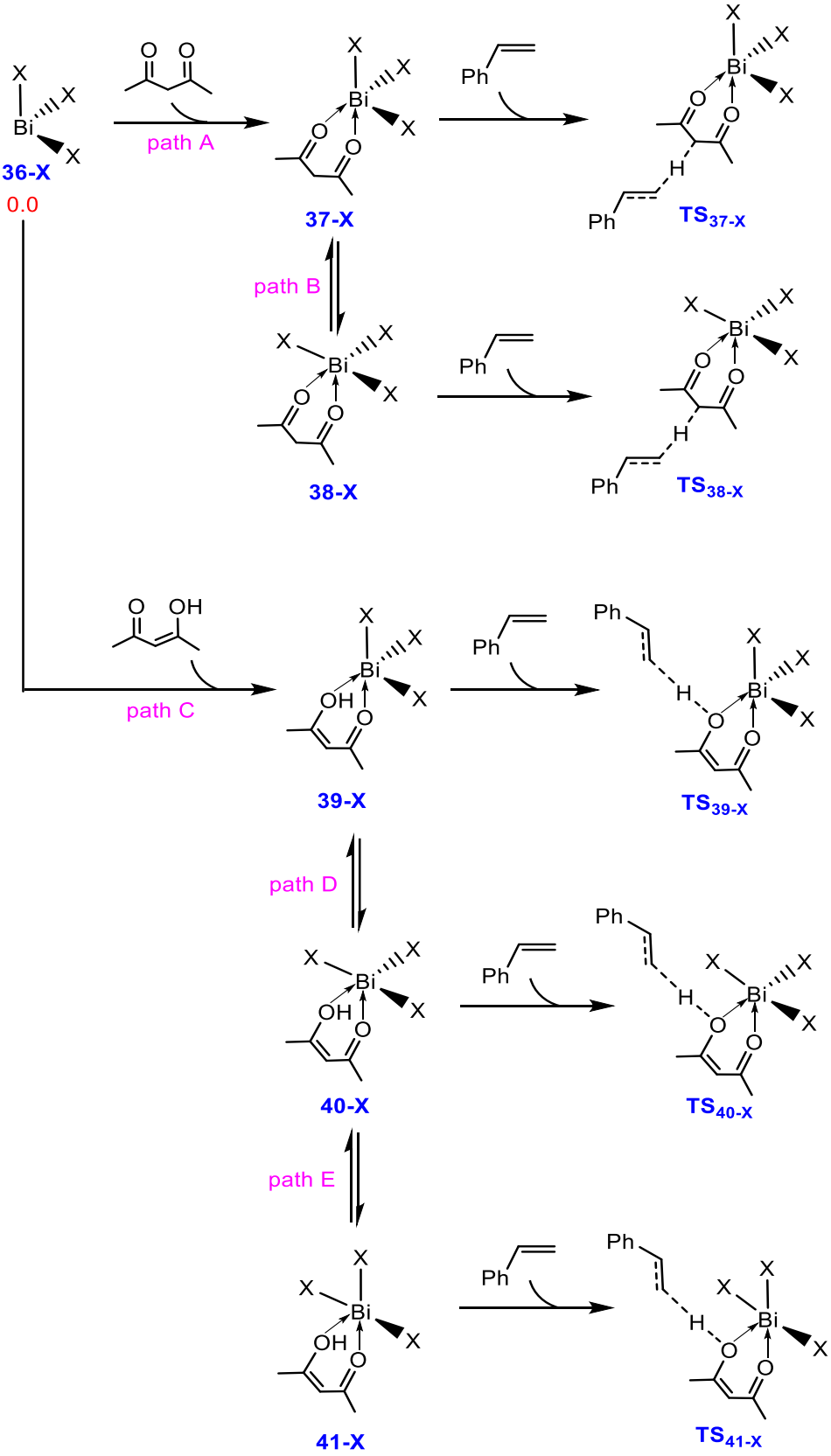

	path A		path B		path C		path D		path E	
X	**37-X**	**TS_{37-X}**	**38-X**	**TS_{38-X}**	**39-X**	**TS_{39-X}**	**40-X**	**TS_{40-X}**	**41-X**	**TS_{41-X}**
Cl	-2.3	37.5	3.5	38.0	4.9	34.0	8.3	34.1	13.1	35.6
Br	-3.2	37.7	3.8	38.1	4.4	34.2	9.1	35.0	13.5	35.7

Scheme 1

(a)

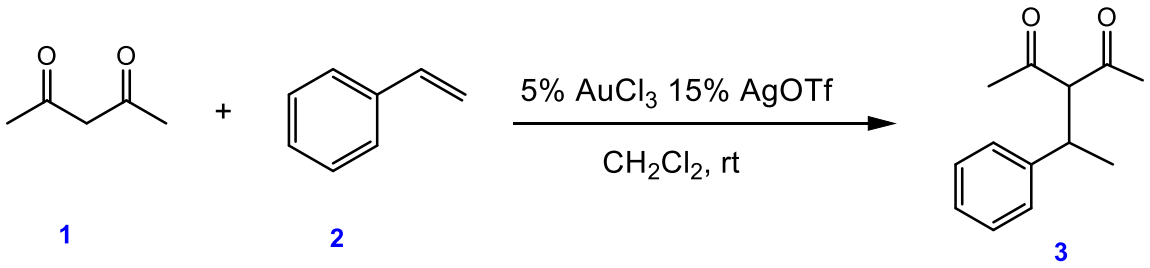

(b)

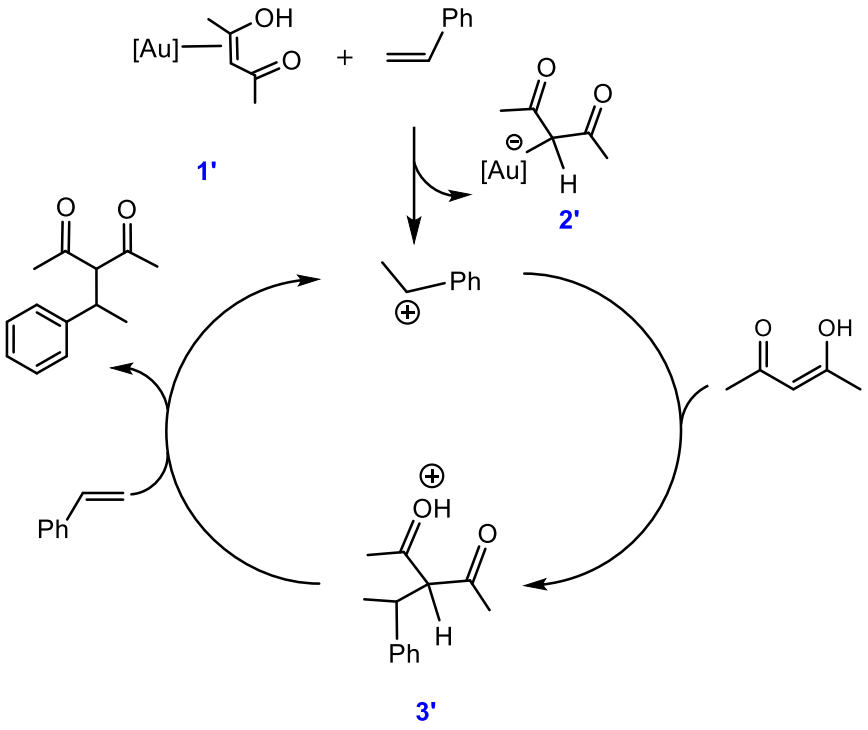

Scheme 2

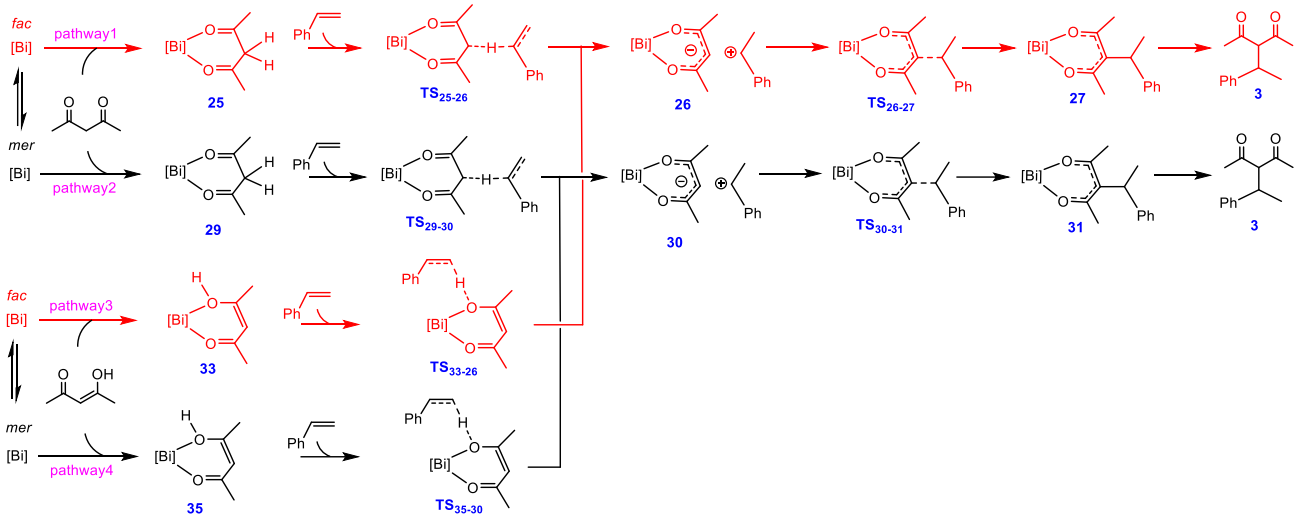
fac
[Bi]
pathway1
mer
[Bi]
pathway2
25
29
Ph
TS25-26
TS29-30
26
30
TS26-27
TS30-31
27
31
3
3
fac
[Bi]
pathway3
mer
[Bi]
pathway4
OH
33
35
TS33-26
TS35-30

Scheme 3

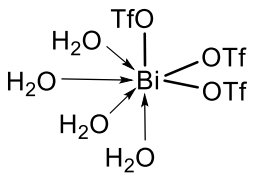

4

0.0

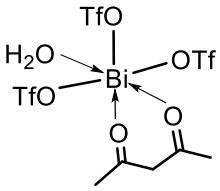

29

-2.2

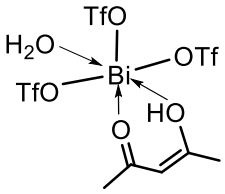

35

0.2

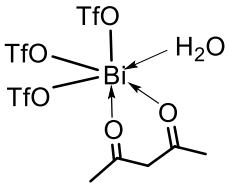

25

2.4

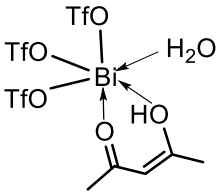

33

3.2

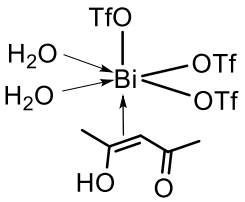

14

15.3

ref. 20

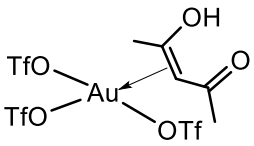

17''

0.0

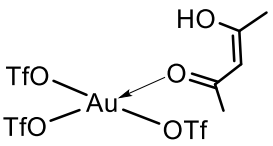

23

12.2

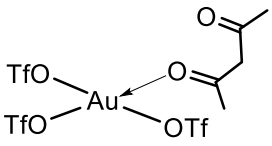

23'

15.8

Figure 1

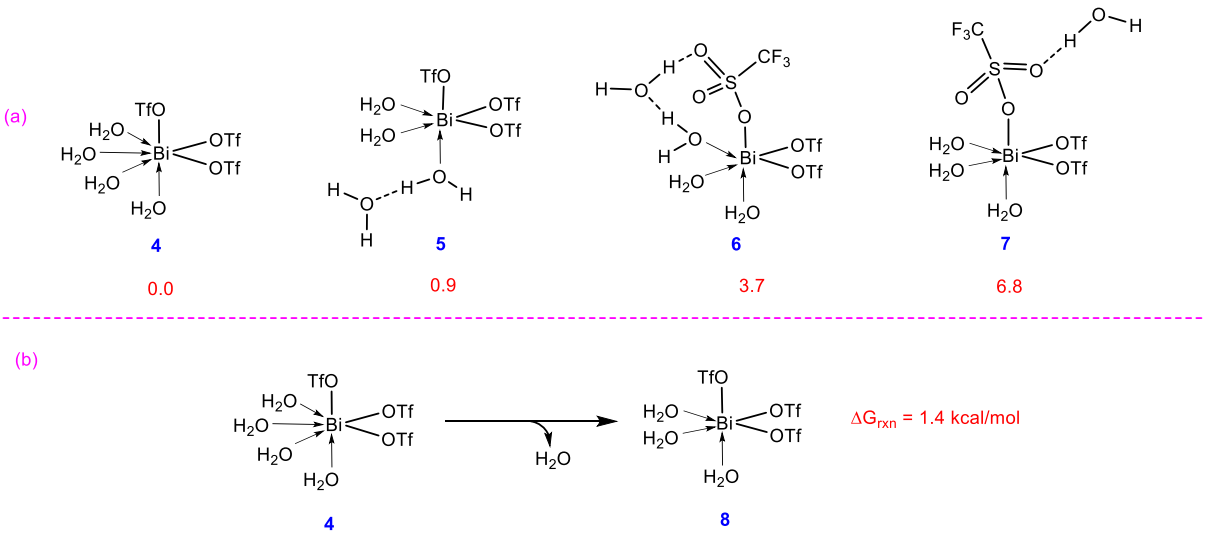
(a)
TfO
H2O
H2O
H2O
H2O
Bi
OTf
OTf
4
0.0
TfO
H2O
H2O
Bi
OTf
OTf
H
O
H
O
H
5
0.9
H
O
CF3
S
O
O
H
O
H
H2O
H2O
Bi
OTf
OTf
6
3.7
F3C
S
O
O
H
O
H
O
H2O
H2O
Bi
OTf
OTf
7
6.8

(b)
TfO
H2O
H2O
H2O
H2O
Bi
OTf
OTf
4
H2O
TfO
H2O
H2O
Bi
OTf
OTf
H2O
8
ΔGrxn = 1.4 kcal/mol

Figure 2

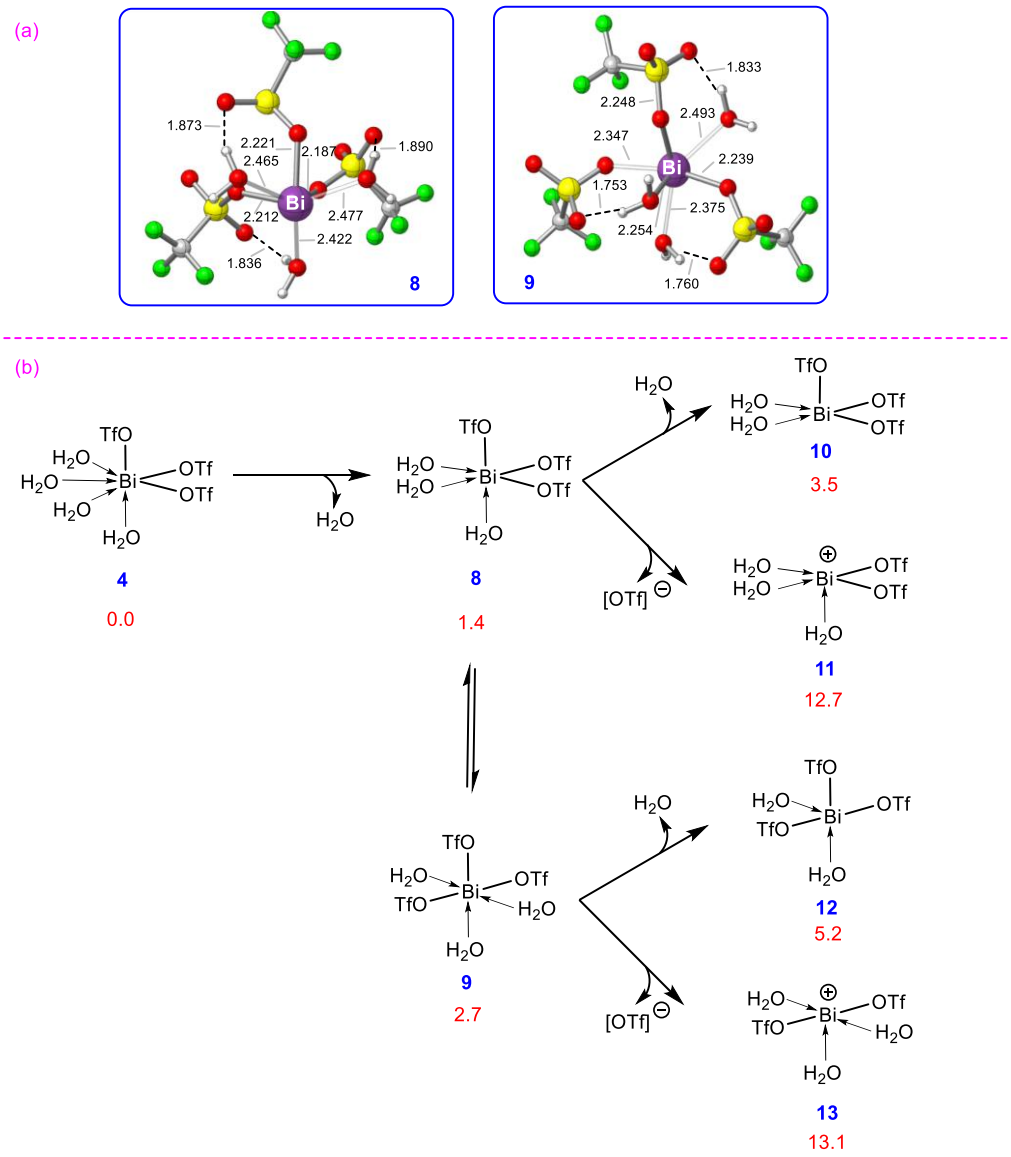
(a)
1.873
2.221
2.465
2.187
1.890
Bi
2.212
2.477
2.422
1.836
8
1.833
2.248
2.493
2.347
Bi
2.239
1.753
2.375
2.254
1.760
9
(b)
TfO
H2O
H2O
Bi
OTf
OTf
H2O
4
0.0
H2O
8
1.4
[OTf]
10
3.5
11
12.7
9
2.7
12
5.2
13
13.1

Figure 3

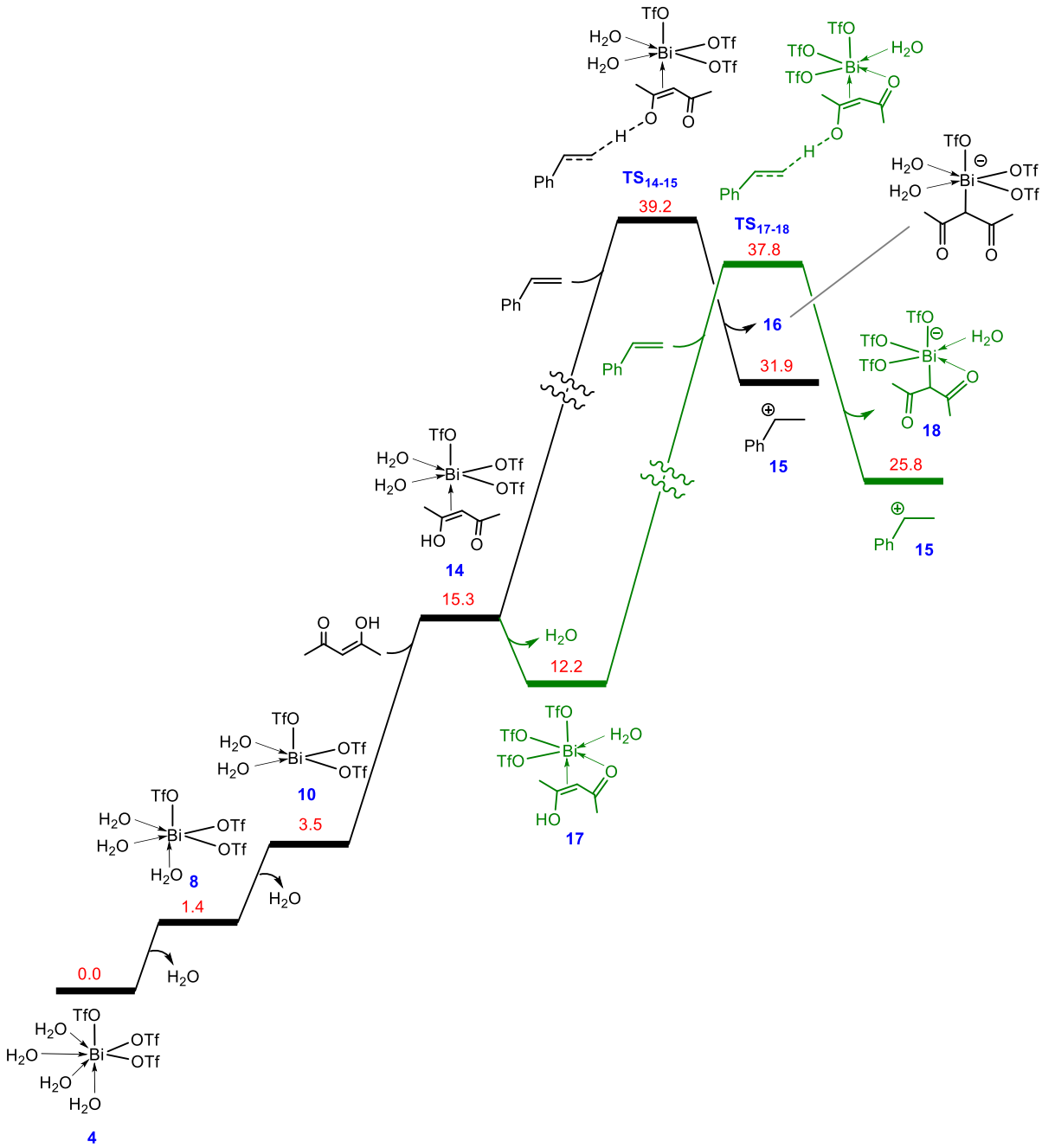
TfO
H2O
H2O
Bi
OTf
OTf
O
H
Ph
TS14-15
39.2
TS17-18
37.8
16
31.9
15
18
25.8
15
14
15.3
OH
HO
H2O
12.2
17
10
3.5
8
1.4
0.0
4

Figure 4

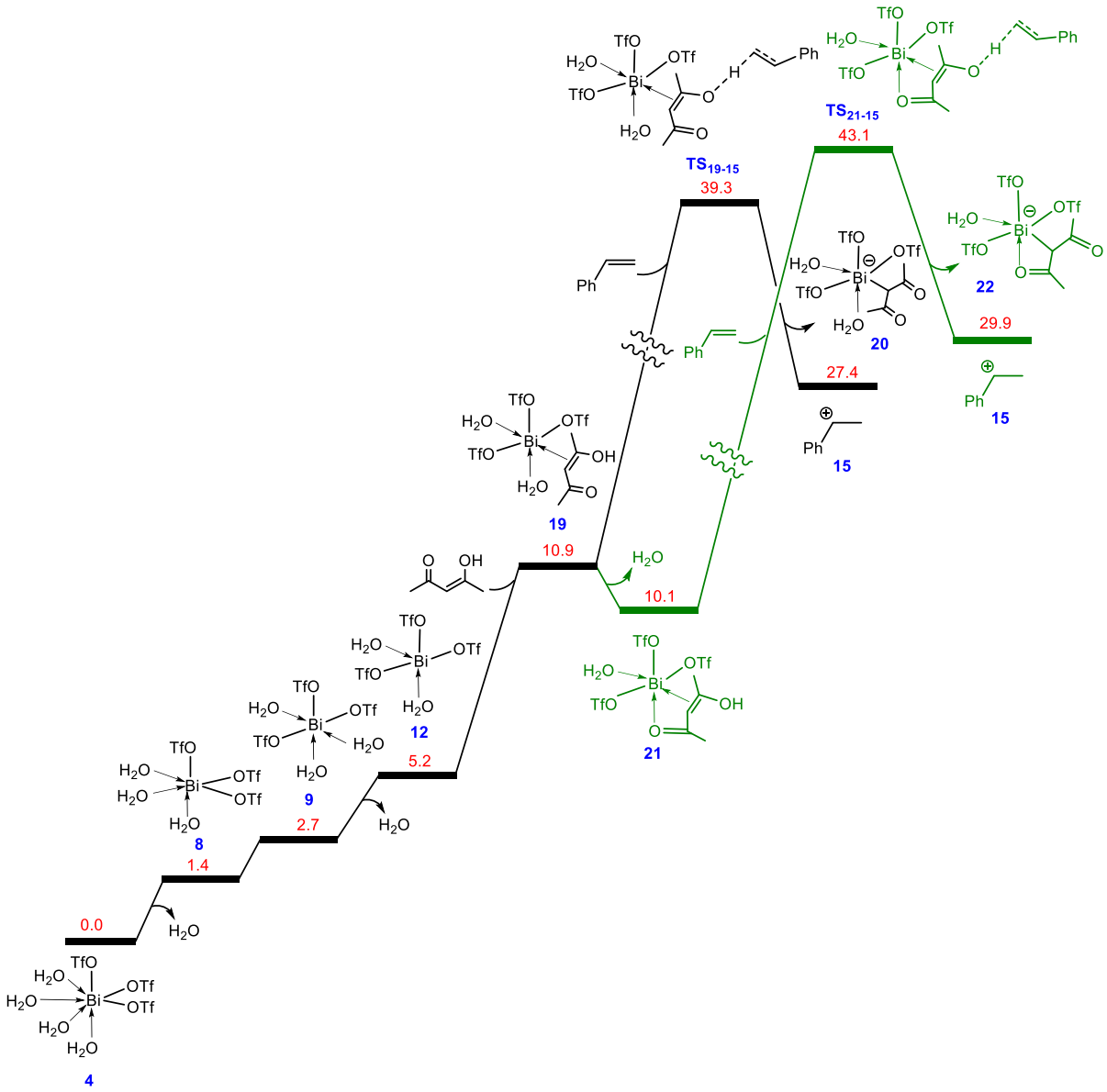
TfO
H2O
OTf
Bi
TfO
H2O
4
0.0
H2O
8
1.4
H2O
9
2.7
H2O
12
5.2
H2O
19
10.9
H2O
10.1
21
TS19-15
39.3
TS21-15
43.1
Ph
20
27.4
15
22
29.9
15
OH
O

Figure 5

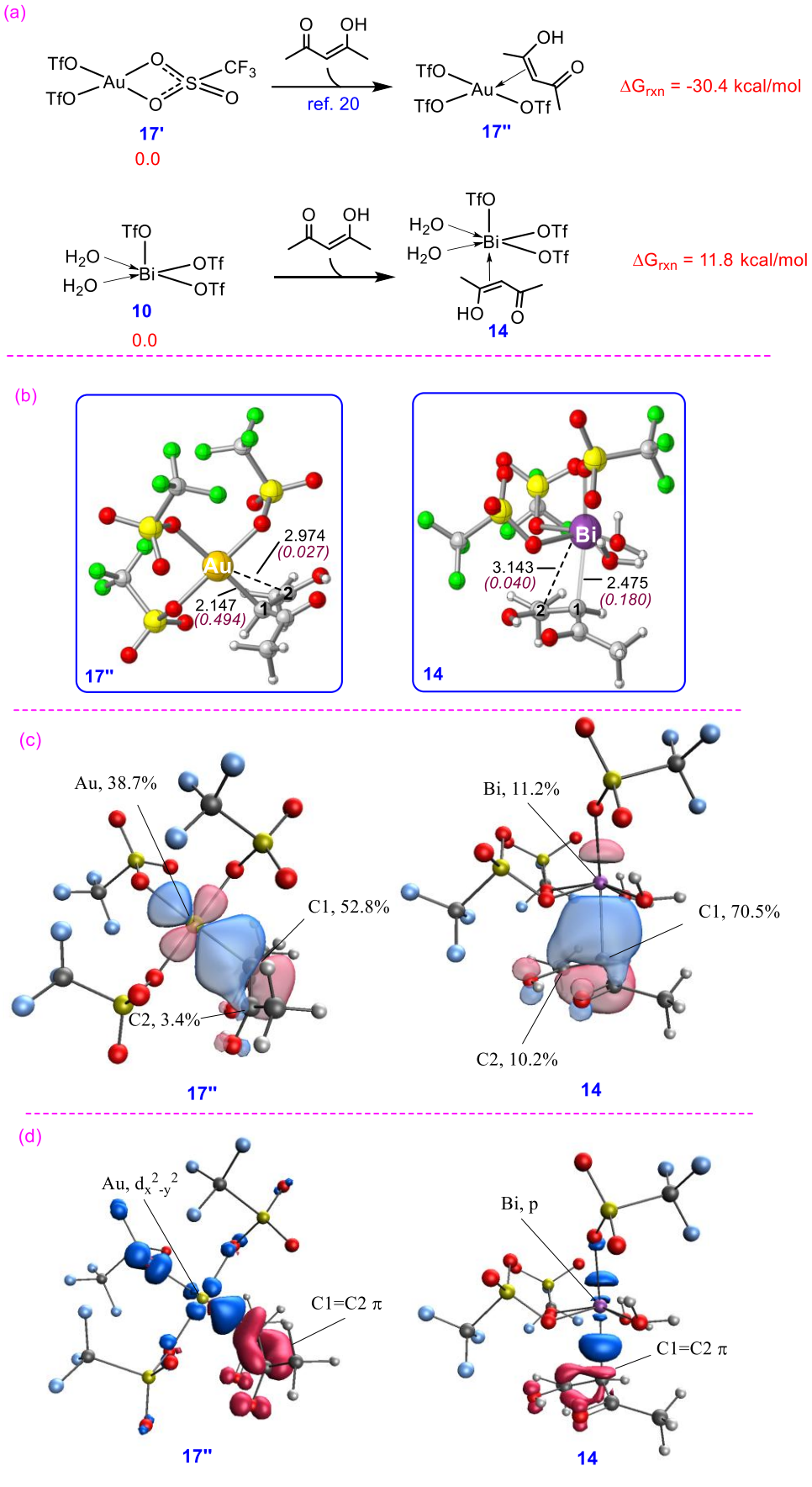
(a)
TfO
TfO
Au
O
S
CF3
O
O
17'
0.0
O
OH
ref. 20
TfO
TfO
Au
OH
O
OTf
17"
ΔGrxn = -30.4 kcal/mol
TfO
H2O
H2O
Bi
OTf
OTf
10
0.0
O
OH
TfO
H2O
H2O
Bi
OTf
OTf
HO
O
14
ΔGrxn = 11.8 kcal/mol
(b)
Au
2.974
(0.027)
2.147
(0.494)
2
1
17"
Bi
3.143
(0.040)
2.475
(0.180)
2
1
14
(c)
Au, 38.7%
C1, 52.8%
C2, 3.4%
17"
Bi, 11.2%
C1, 70.5%
C2, 10.2%
14
(d)
Au, dx2-y2
C1=C2 π
17"
Bi, p
C1=C2 π
14

Figure 6

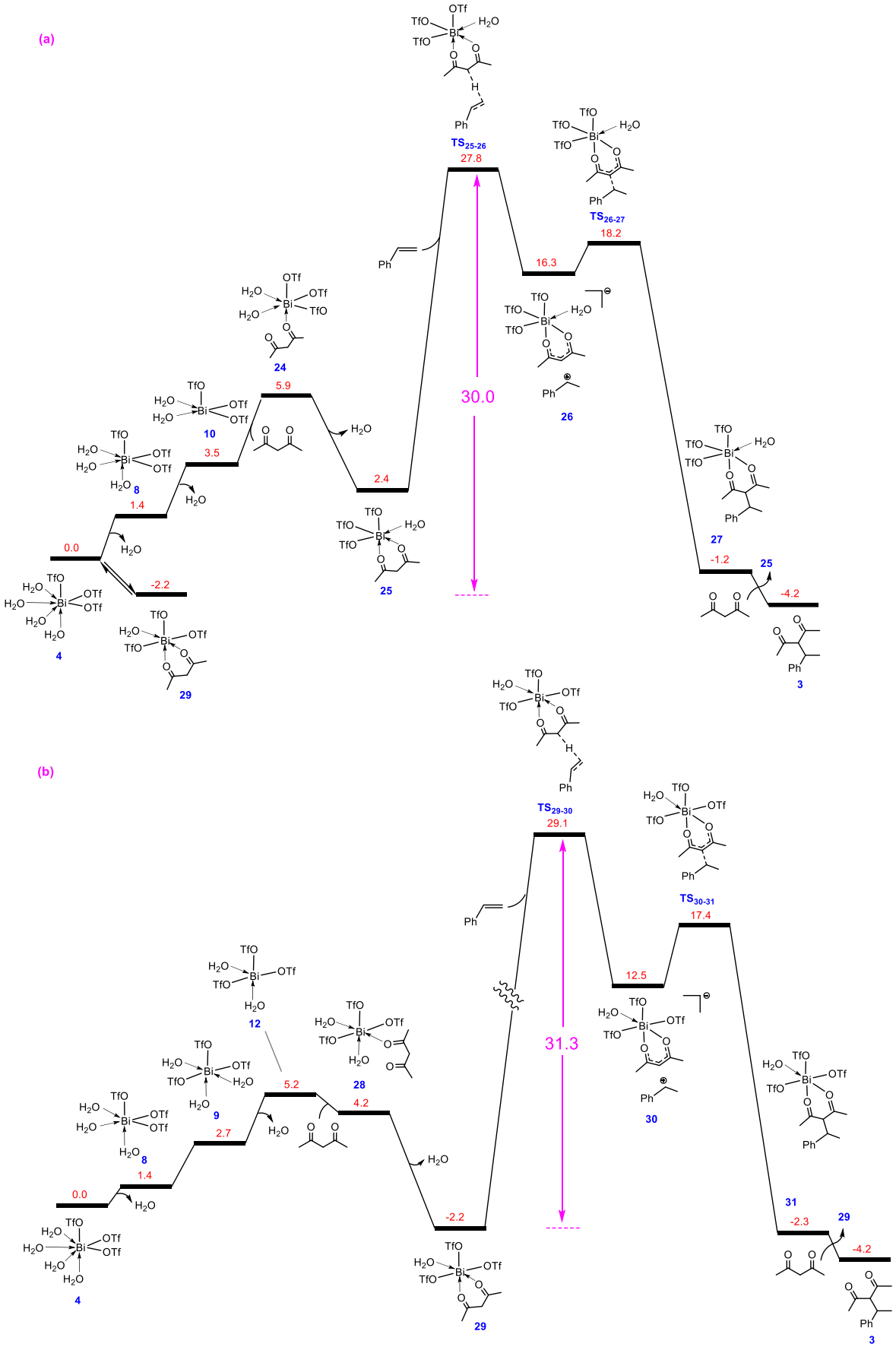
(a)
TS25-26
27.8
TS26-27
18.2
16.3
30.0
24
5.9
10
3.5
8
1.4
0.0
4
29
2.4
25
26
27
-1.2
25
-4.2
3
(b)
TS29-30
29.1
TS30-31
17.4
12.5
31.3
12
5.2
28
4.2
9
2.7
8
1.4
0.0
4
-2.2
29
30
31
-2.3
29
-4.2
3

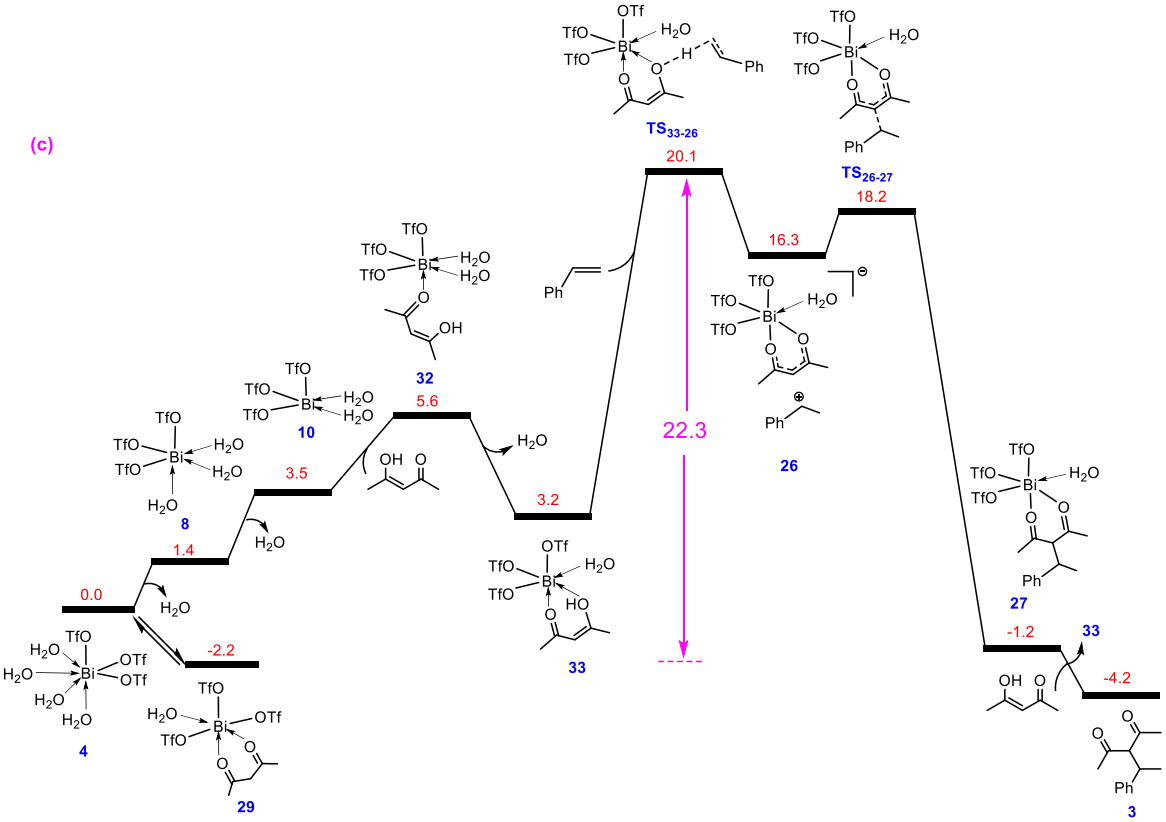
(c)
TS33-26
20.1
TS26-27
18.2
16.3
22.3
32
5.6
10
3.5
8
1.4
0.0
-2.2
4
29
3.2
33
26
27
-1.2
33
-4.2
3

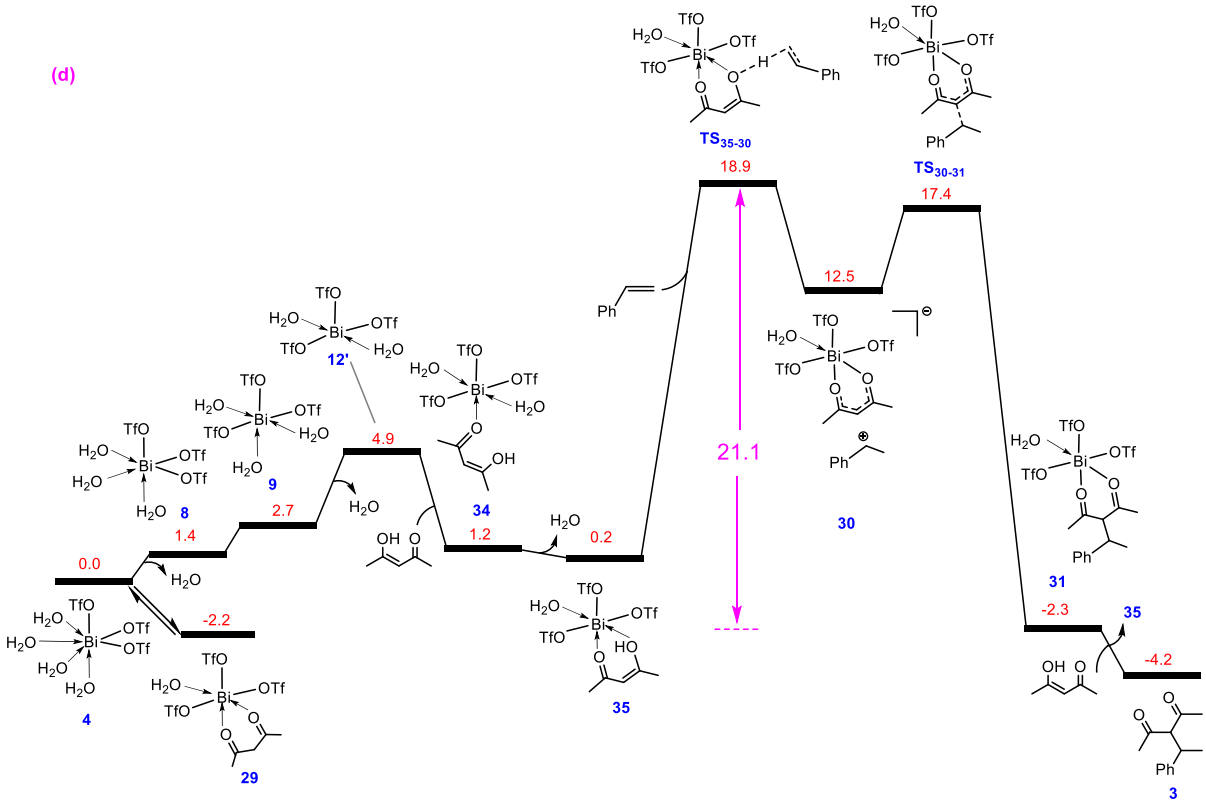
(d)
TS35-30
18.9
TS30-31
17.4
12.5
21.1
12'
4.9
9
8
2.7
1.4
0.0
-2.2
4
29
34
1.2
0.2
35
30
31
-2.3
35
-4.2
3

Figure 7

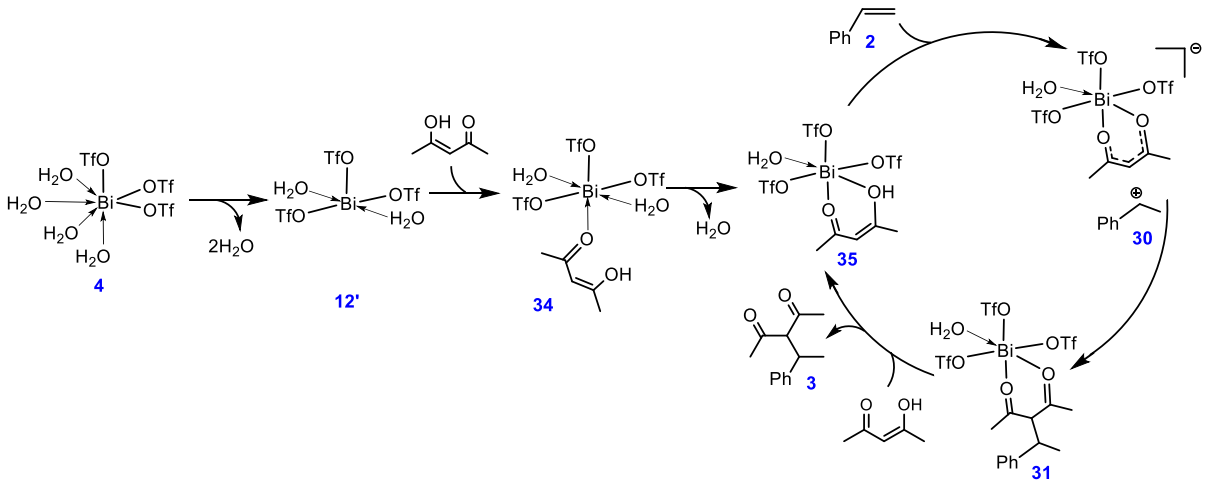

Figure 8

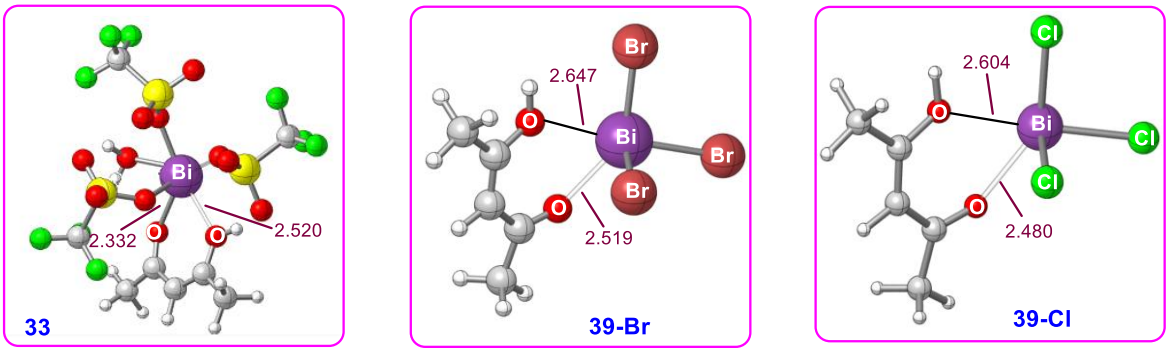
Bi
O
O
2.332
2.520
33
Br
2.647
O
Bi
Br
Br
O
2.519
39-Br
Cl
2.604
O
Bi
Cl
Cl
O
2.480
39-Cl

Scheme 1. (a) Hydroalkylation facilitated by $AuCl_3$/AgOTf developed by Li and coworkers [11]. (b) Proposed benzylic carbocation mechanism elucidated by Ariafard and coworkers [20].

Scheme 2. Different possible mechanistic pathways leading to hydroalkylation product **3** by the reaction of enol and ketone tautomers of acetylacetone with the *fac* and *mer* isomers of $Bi(OTf)_3(H_2O)_4$.

Scheme 3. Stability comparison between the different bismuth and gold complexes. Free energies calculated by SMD/M06-2X/def2-TZVP//SMD/M06-2X/LANL2DZ(d),6-31G(d) level of theory in nitromethane are given in kcal/mol.

Figure 1. (a) Calculated stability of different isomers of $Bi(OTf)_3(H_2O)_4$. (b) Reaction free energy for the dissociation of one water molecule from **4**. Free energies calculated at SMD/M06-2X/def2-TZVP//SMD/M06-2X/LANL2DZ(d),6-31G(d) level of theory in nitromethane are given in kcal/mol.

Figure 2. (a) Optimised structures for the most stable conformers of the *fac* and *mer* isomers of complex $Bi(OTf)_3(H_2O)_3$. (b) Reaction free energies for the dissociation of the triflate and water ligands from **4**. Free energies calculated by SMD/M06-2X/def2-TZVP//SMD/M06-2X/LANL2DZ(d),6-31G(d) level of theory in nitromethane are given in kcal/mol, and selected bond distances in Å.

Figure 3. Calculated free energy profile for the hydroalkylation reaction via benzylic carbocation mechanism where the enol tautomer of acetylacetone coordinates to coordinatively unsaturated species **10**. Free energies calculated by SMD/M06-2X/def2-TZVP//SMD/M06-2X/LANL2DZ(d),6-31G(d) in nitromethane are given in kcal/mol.

Figure 4. Calculated free energy profile for the hydroalkylation reaction via benzylic carbocation mechanism where the enol tautomer of acetylacetone coordinates to coordinatively unsaturated species **12**. Free energies calculated by SMD/M06-2X/def2-TZVP//SMD/M06-2X/LANL2DZ(d),6-31G(d) level of theory in nitromethane are given in kcal/mol.

Figure 5. (a) Reaction free energies for the coordination of enol tautomer to the Au(III) complex **17′** and the Bi(III) complex **10** [20]. Free energies calculated by SMD/M06-

2X/def2-TZVP//SMD/M06-2X/LANL2DZ(d),6-31G(d) level of theory in nitromethane are given in kcal/mol. (b) Optimised structures for **14** and **17′′**. Selected bond distances (black values) and Wiberg bond indexes (brown values) are given in Å. (c) Spatial plots for NLMO orbitals associated with the enol→M interactions in complexes **14** (M = Bi) and **17''** (M = Au). (d) Contour plots of NOCV for orbital interaction of the enol C=C orbital with the $d_{x^2-y^2}$ orbital of Au in **17''** and a p orbital of Bi in **14**. The charge transfer occurs from the red orbitals to the blue orbitals.

Figure 6. Calculated free energy profiles for the hydroalkylation reaction via the four different pathways outlined in Scheme 2. Free energies calculated by SMD/M06-2X/def2-TZVP//SMD/M06-2X/LANL2DZ(d),6-31G(d) level of theory in nitromethane are given in kcal/mol.

Figure 7. Catalytic cycle proposed by the DFT calculations for the hydroalkylation of styrene with acetylacetone.

Figure 8. Optimised structures for **33**, **39-Br** and **39-Cl**. Selected bond distances are given in Å.

Graphical abstract

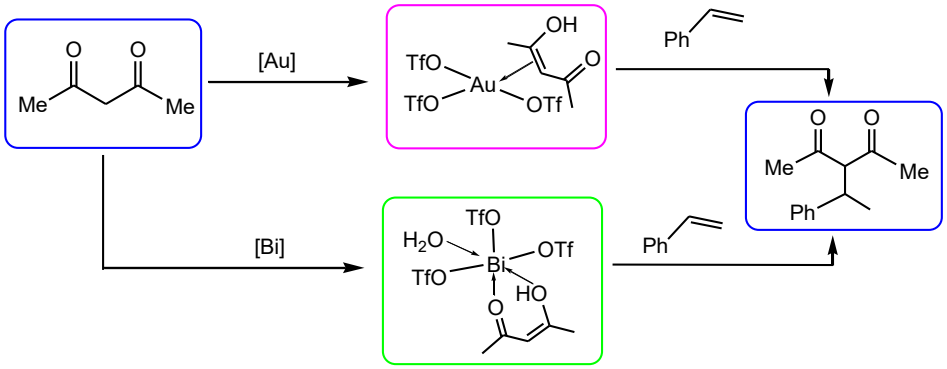

Same product, different mechanisms